IEEE Access
Multidisciplinary | Rapid Review | Open Access Journal

Received 2 November 2022, accepted 21 November 2022, date of publication 24 November 2022,
date of current version 6 December 2022.

Digital Object Identifier 10.1109/ACCESS.2022.3224776

RESEARCH ARTICLE

Air-to-Ground Large-Scale Channel Characterization by Ray Tracing

MENGAN SONG[1], (Student Member, IEEE), YIMING HUO[2], (Senior Member, IEEE), ZHONGHUA LIANG[1], (Senior Member, IEEE), XIAODAI DONG[2], (Senior Member, IEEE), AND TAO LU[2], (Member, IEEE)

[1]School of Information Engineering, Chang'an University, Xi'an, Shanxi 710064, China
[2]Department of Electrical and Computer Engineering, University of Victoria, Victoria, BC V8P 5C2, Canada

Corresponding authors: Xiaodai Dong (xdong@ece.uvic.ca) and Tao Lu (taolu@ece.uvic.ca)

The work of Mengan Song and Zhonghua Liang was supported in part by the Natural Science Basic Research Project in Shaanxi Province of China under Grant 2020JM-242 and Grant 2021JM-185, and in part by the National Natural Science Foundation of China under Grant 61871314. The work of Yiming Huo, Xiaodai Dong, and Tao Lu was supported by the Natural Sciences and Engineering Research Council of Canada (NSERC) under Grant RGPIN-2018-03778.

ABSTRACT Through ray tracing simulation on three-dimensional (3D) urban environments, we characterize air-to-ground (A2G) channels for 5G and beyond wireless communications. In this study, we review four types of elevation angle-dependent probability of line-of-sight (LoS) expressions according to building distribution types. With channel characterization data extracted from the ray tracing (RT) simulation, LoS probability versus elevation angle agrees better with the elevation angle-dependent probability expressions of LoS that assumes the buildings are randomly distributed. Furthermore, we provide a more accurate LoS probability expression that enables better curve-fitting for the LoS probability data obtained from RT simulations. In addition, the A2G channel parameters such as LoS and non-line-of-sight (NLoS) channel path loss exponents (PLEs) and the shadow fading with UAV altitudes are obtained in four typical and realistic urban environments. The LoS PLEs increase slowly with the height of the UAV, while the NLoS one decreases significantly with the increase of the UAV height.

INDEX TERMS Unmanned aerial vehicle (UAV), line-of-sight (LoS) probability, air-to-ground (A2G), ray tracing (RT), realistic urban environments, path loss exponent (PLE).

I. INTRODUCTION

In recent years, with the maturity of technology and the significant cost reduction in manufacturing, unmanned aerial vehicles (UAVs) have been widely used in various fields from forest fire prevention [1], environmental monitoring, maritime communications [2], agricultural plant protection, geological prospecting, power line inspection [3] to film and television aerial photography [4], etc. In telecommunication, due to the inherent properties of UAVs such as high deployment flexibility, mobility and fast altitude-changing capability, UAVs are indispensable in future wireless networks [5], [6], [7]. In a cellular network, UAVs play critical roles in two categories: cellular-connected and wireless communications assisting UAVs [8]. In the former category, UAVs are new aerial users that access the cellular network from the sky. In the latter one, UAVs are new aerial communications base stations (BSs) and relays to assist terrestrial wireless communications by providing data access from the sky [9], [10]. In an urban environment where a UAV is deployed as a base station, line-of-sight (LoS) links between the UAV and ground nodes are stochastically blocked by ground obstacles such as buildings and trees. There is a group of LoS probabilistic models [11], [12], [13] which can predict the probability of LoS link between the UAV and the ground users. They provide excellent solutions for handling some channel parameters such as path loss and shadow fading for LoS and NLoS cases separately, which leads to the further development of the LoS probabilistic models. The mathematical expressions of these models are related to the urban environmental parameters as well as the transmitter-receiver relative position such as horizontal distance, elevation angle, and so on.

The associate editor coordinating the review of this manuscript and approving it for publication was Wei-Wen Hu.

In addition, some LoS probabilistic models consider the frequency of radio waves as a parameter according to the first Fresnel zone [14], [15]. Some of these models have the same type of urban environmental parameters, while others have different types. The comparison of models based on the same type of urban environmental parameters is one of the motivations of this paper. In particular, a new channel model wherein the effects of mobility and shadowing are simultaneously considered has been proposed in [16]. Moreover, authors have conducted experiments and analyzed the performance of a UAV-based communication system operating in a shadowed double-scattering channel. Furthermore, it is critical to precisely measure and model the shadowing effects which are believed to be correlated with the drone body and various antenna placements [17], and also the human body and the user orientation [18].

Among the above-mentioned expressions of LoS probability, there are three expressions based on the same type of urban environmental parameters. The parameters are given as follows:

1) α: the ratio of the land area covered by buildings to the total land area;
2) β: the average number of buildings per unit area;
3) γ: the scale parameter for a Rayleigh distributed building height.

The first of these three expressions was proposed by the International Telecommunication Union (ITU) for traditional terrestrial communications [11]. Since it is generic and valid for transmitter and receiver at any height, it can also be used for UAV Communications. The altitude-dependent probability expression of LoS from ITU [11] can also be extended as an elevation angle-dependent form as shown in (5), which forms one of several contributions in this paper. The extended-expression is referred to as the ITU elevation angle-dependent probability expression of LoS. The second expression is a simplified elevation angle-dependent probability expression of LoS proposed by A. Al-Hourani et al. [12] based on [11]. The expression is $\mathbf{P}(\text{LoS}, \theta) = \frac{1}{1+a\exp(-b[\theta-a])}$, where θ is the elevation angle of the UAV, a and b are the S-curve fitting parameters directly to the environment parameters α, β and γ. This probability expression of LoS is applied to optimize the UAV height to achieve the maximum wireless coverage on the ground. It is in closed form with respect to the elevation angle and the urban statistical parameters which significantly ease the calculation of the LoS probability. From the application perspective, this simplified expression is more advantageous than the ITU expression, which reduces the calculation complexity. From the perspective of analysis, it is more suitable to use the ITU expression, which is more general than the second simplified expression, because it uses the original urban environmental parameters rather than the fitted new parameters such as parameters a and b in [12]. The third expression of LoS probability proposed in [13] is based on the random distribution of building locations wherein the location and height of the buildings follow the 2D homogeneous Poisson point process (PPP) and Rayleigh distribution, respectively. One of the contributions of this paper is to derive a new LoS probability expression based on the LoS probability expression in [13]. In our derived expression, the locations of the buildings also follow a Poisson point process, but the heights of the buildings follow a log normal distribution.

In addition to the three LoS probability expressions based on the same type of urban environmental parameters introduced above, there are also some expressions that use different types of urban environmental parameters. In [19], the author presents a LoS probability predicting expression in different urban environments based on five urban environment parameters. These parameters include α and β mentioned above, and the other three parameters are the average and standard deviation of the height of the buildings in the selected area and the average radius of the building base. It is worth mentioning that the author simplified the building as a cylinder whose position follows a PPP on a 2-dimensional plane. In [20], the authors proposed a LoS probability predicting expression which requires five or more urban environment parameters. The urban environment is treated as a regular urban grid deployment of building blocks captured by a Manhattan Poisson line process (MPLP) with generally distributed building heights. Both expressions have more urban environment parameters and are therefore more complex than the three expressions mentioned above. The motivation of this paper is to compare and verify the first three expressions that are based on environmental parameters of the same type. Since the second of the three previously mentioned expressions is a simplified version of the first, and the precision difference between the two is not significant, in this paper we focus on comparing and verifying the first and third expressions that predict the probability of LoS. For convenience, we list the LoS probability expressions described above in Table 1.

Reference [21] briefly summarizes and compares some existing LoS probability expressions, but it lacks simulation verification based on real urban environments. Authors in [22] used a GPU-based ray launching algorithm to conduct the verification of the altitude-dependent LoS probability expression derived from [12] in three different cities, but there is a lack of comparison with other LoS probability expressions. To the best of our knowledge, there is a lack of experimental verification for the ITU elevation angle-dependent probability expression of LoS based on the evenly spaced buildings assumption, and the elevation angle-dependent probability expressions of LoS based on the assumption of randomly distributed buildings. Therefore, to understand the suitability of the four formulas applied to realistic propagation environments, we conduct further research with primary contributions unfolded as in the following aspects:

1) First, we deliver a thorough investigation of the existing LoS probability expressions for A2G channels in urban environments. Furthermore, we compare, modify, and verify the first, third, and fourth LoS probability expressions in Table 1 plus one LoS expression

TABLE 1. Summary of line-of-sight probability expressions for UAV communications.

	Scenarios	Roles of UAVs	Location / Height of buildings	Number of the environment parameters
1st, [11]	Terrestrial / A2G	Wireless communications assisting UAVs	Evenly spaced / Rayleigh distribution	3
2nd, [12]	A2G	Wireless communications assisting UAVs	Evenly spaced / Rayleigh distribution	3
3rd, [13]	A2G	Wireless communications assisting UAVs	PPP / Rayleigh distribution	3
4th, [19]	A2G / A2A	Cellular-connected UAVs / Wireless communications assisting UAVs	PPP / Log-Normal distribution	5
5th, [20]	A2G	Cellular-connected UAVs	MPLP / Uniform, Exponential, Rayleigh distribution	≥ 5

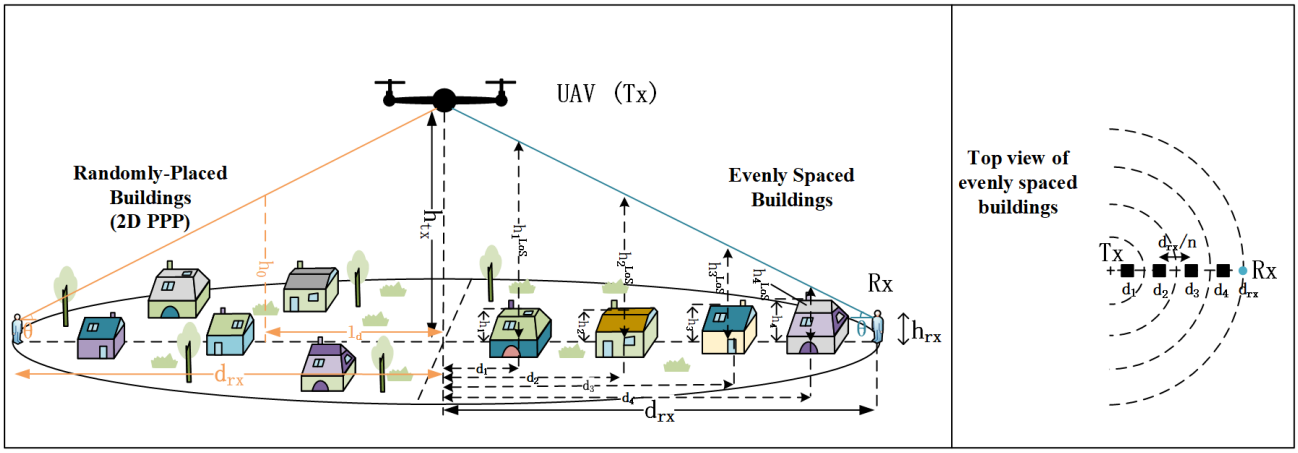

FIGURE 1. Distribution of buildings corresponding to the two probability expressions of LoS.

derived based on [13] with four types of realistic urban environment-based ray tracing (RT) simulations.

2) Second, we conduct a more accurate curve-fitting for the LoS probability data obtained from RT simulations and then derive an elevation angle-dependent LoS probability expression.
3) Third, based on the collection and analysis of a large amount of extracted RT data, we characterize the A2G channel in terms of LoS and non-line-of-sight (NLoS) channels' path loss exponents (PLEs) and the shadow fading parameters, with altitudes of the UAV varied over a practical range of interest.

The remainder of this article is organized as follows. Section II revisits the probability of LoS in A2G channels with two major types of building distribution. Section III presents all the details of RT-based simulations on top of real-world urban environments. Furthermore, Section IV presents and analyzes all extracted data from simulations, and further unveils the critical relationships in A2G channels. Section V concludes the paper and discusses possible future work.

II. PROBABILITY OF LoS IN A2G CHANNELS

In this section, we review the three existing LoS probability expressions and the one we derived for A2G channels in urban environments. For the three existing LoS probability expressions, the first one assumes that the distances between buildings are uniform and the building height is a random variable, while the other two assume both two parameters are random. Specifically, the location of the buildings in the second expression [13] and the third one [19] are both modeled as random points following the Poisson point process (PPP). And the heights of the buildings in these two LoS probability expressions conform to Rayleigh and log-normal distribution, respectively. It is worth noting that the second LoS probability expression is derived based on 1D inhomogeneous PPP, which essentially calculates the probability that there are no points on the horizontal distance between the transmitter and receiver.

In contrast, the third one is derived based on 2D PPP, which calculates the probability of a region between the transmitter and receiver being void of points. Furthermore, we enrich our comparison by deriving a LoS probability expression based on a log-normal distribution of building heights from the second LoS probability expression. Therefore, in this paper, we compare four LoS probability expressions and verify them based on four types of realistic urban environment-based ray tracing (RT) simulations. The corresponding building distribution scenarios are shown in Fig. 1.

To summarize this section, we first present and review the elevation angle-dependent versions of three existing LoS probability expressions. Then, we derive a LoS probability expression based on the log-normal distribution of building heights. For the overall architecture, we divide this section into two subsections according to the distribution type of the building locations. The first one is based on buildings

distributed uniformly, while the second one is on top of the buildings distributed by the Poisson point process.

A. EVENLY SPACED RANDOM-HEIGHT BUILDINGS

The probability of LoS based on evenly spaced buildings is to calculate the probability that the height of the building is smaller than that of the LoS ray at the building location [11]. There are two key types of heights: first, the height of the building, h_i; second, between the transmitter and the receiver, there is the height of the LoS ray h_i^{LoS} at the i-th building location as illustrated in Fig. 1. Here, i specifically represents the index of the building within the range of the transmitter and the receiver projected on the ground. The expression in [11] assumes h_i follows the Rayleigh distribution i.e.,

$$P_{h_i}(h) = \frac{h}{\gamma^2} e^{-\frac{h^2}{2\gamma^2}}, \tag{1}$$

where γ is the scale parameter. Meanwhile, the height of the LoS ray at the building coordinate h_i^{LoS} can be expressed as

$$h_i^{LoS} = h_{tx} - \frac{d_i\,(h_{tx} - h_{rx})}{d_{rx}}, \tag{2}$$

where h_{tx} and h_{rx} are the altitudes of the transmitter and receiver, both measured from above the ground, and d_i and d_{rx} are the horizontal distances from the transmitter to the i-th building and to the receiver respectively. According to (1) and (2), the probability that h_i is smaller than the height of the LoS ray at this building location can be obtained as

$$P(h_i < h_i^{LoS}) = \int_0^{h_i^{LoS}} P(h)dh = 1 - e^{-\frac{(h_i^{LoS})^2}{2\gamma^2}}. \tag{3}$$

We use P_i^{LoS} to denote $P(h_i < h_i^{LoS})$, which leads to the probability of the LoS ray at the receiver given by

$$P_{LoS} = \prod_{i=0}^{n-1} P_i^{LoS}, \tag{4}$$

where $i \in \{0, \ldots, n-1\}$, α is defined as the ratio of the land area covered by buildings to the total land area, and β is defined as the average number of buildings per unit area. And $n = \lfloor d_{rx}\sqrt{\alpha\beta} \rfloor$ is the number of buildings between the transmitter and the receiver. Here, $\sqrt{\alpha\beta}$ is the number of buildings that the rays pass through per unit length. Multiply it by d_{rx} and truncate it to an integer to obtain the number of buildings between the receiver and the transmitter. And d_{rx} and n can be used to obtain the distance from the transmitter to the i-th building $d_i = (i + 1/2)\frac{d_{rx}}{n}$, $i \in \{0, \ldots, n-1\}$.

So far, the above LoS probability expression is used to calculate the LoS probability between the traditional terrestrial transmitter and receiver. Next, we discuss the probability of LoS between the transmitter in the air and the receiver on the ground in terms of the elevation angle of the UAV. When treating the UAV in the air as the transmitter, the height of the receiver on the ground is sufficiently small to be ignored for simplicity in this work. The elevation angle of the UAV relative to the ground receiver is represented by θ, and the height of transmitter h_{rx} can be calculated as $h_{tx} = d_{rx} \tan\theta$. According (1) to (4), the relationship between θ and the LoS probability can be derived as (5), shown at the bottom of the next page.

It is worth noting that when the value of n is greater than or equal to 2, that is, when $n = \lfloor d_{rx}\sqrt{\alpha\beta} \rfloor \geq 2$, (5) is valid, and the corresponding value range of d_{rx} can be deduced as $d_{rx} \geq \frac{2}{\sqrt{\alpha\beta}}$.

B. RANDOMLY PLACED BUILDINGS WITH RANDOM HEIGHT

1) ONE-DIMENSIONAL PPP LoS EXPRESSION BASED ON THE RAYLEIGH DISTRIBUTION OF BUILDING HEIGHTS

The locations of the buildings in the LoS probability expression from [13] are modeled as random points following the Poisson point process (PPP), while the buildings' heights conform to the Rayleigh distribution. The density parameter of the PPP is defined as $\alpha\beta$, and its unit is the number of buildings per square kilometer. In terms of the thinning property of PPP, the distribution of the buildings that block the LoS ray conforms to 1D inhomogeneous PPP. The relationship between the LoS probability and the UAV elevation angle is derived as

$$P_{LoS2}(\theta) = \exp\left(-\sqrt{\frac{\alpha\beta\pi}{2}}\frac{\gamma}{\tan(\theta)}\,\mathrm{erf}\left(\frac{d_{rx}\tan(\theta)}{\sqrt{2}\gamma}\right)\right), \tag{6}$$

where $\mathrm{erf}(\cdot)$ is the error function.

2) ONE-DIMENSIONAL PPP LoS EXPRESSION BASED ON THE LOG-NORMAL DISTRIBUTION OF BUILDING HEIGHTS

In this paragraph, we derive an elevation angle-dependent LoS probability expression assuming that building heights follow a log-normal distribution. Its cumulative distribution function is given by:

$$F(H) = \frac{1}{2} + \frac{1}{2}\,\mathrm{erf}\left[\frac{\ln H - \mu_0}{\sqrt{2}\sigma_0}\right], \tag{7}$$

where H denotes the random variable height, and μ_0 and σ_0 are the mean and standard deviation of the building heights' logarithm which is calculated as follows:

$$\mu_0 = \ln\left(\frac{m_0}{\sqrt{1 + \frac{v_0}{m_0^2}}}\right), \quad \sigma_0^2 = \ln\left(1 + \frac{v_0}{m_0^2}\right), \tag{8}$$

where m_0 and v_0 represent the mean and variance of the building heights. Furthermore, we model the buildings as random points following a Poisson point process (PPP) with a density $\mu = \alpha\beta$. In terms of the thinning property of PPP, the distribution of the buildings that block the LoS ray conforms to 1D inhomogeneous PPP. We are interested in the probability that there is no building (between the transmitter and receiver) higher than the direct ray between the Tx and Rx. The geometric relationship between the UAV and the ground receiver is shown in Fig. 1 where h_0 is the height of the LoS ray above a specific ground location, l_d is the horizontal distance from this location to the UAV, d_{rx} denotes the horizontal distance from the UAV to a ground receiver and θ is the elevation angle

wherein $\tan(\theta) = \frac{h_{tx}-h_{rx}}{d_{rx}}$. The probability of the buildings above h_0 is the complementary cumulative distribution function (CCDF) of h_0 which is shown as follows:

$$G(h_0) = 1 - F(h_0) = \frac{1}{2} - \frac{1}{2}\,\mathrm{erf}\left[\frac{\ln h_0 - \mu_0}{\sqrt{2}\sigma_0}\right]. \quad (9)$$

Therefore, the density of the buildings above h_0 located at a horizontal distance d_{rx} between the transmitter and a ground receiver is expressed in (10), as shown at the bottom of the next page. According to the void probability of the thinned PPP, the LoS probability can be derived as (11), shown at the bottom of the next page, wherein $h_0 = (d_{rx} - l_d)\tan(\theta) + h_{rx}$, θ represents the elevation angle of UAV, h_{rx} is the altitude of the ground receivers, which are all set to 1.5 meters. Furthermore, the elevation angle-dependent LoS probability can be expressed as (12), shown at the bottom of the next page, wherein erf(·) is the error function.

3) TWO-DIMENSIONAL PPP LoS EXPRESSION BASED ON THE LOG-NORMAL DISTRIBUTION OF BUILDING HEIGHTS

The location of the buildings in the LoS probability expression from [19] is modeled as random points following the Poisson point process (PPP) with density β [building /km^2]. And buildings are represented as cylinders with a fixed radius r_0 and a random height H following the log-normal distribution. The LoS expression is derived by using the void probability of the thinned PPP, i.e., the probability of a region R to be void of points is $\exp(-\lambda|R|)$ where λ is the density of the points [19] equals β and $|\cdot|$ is the area measure. The relationship between the LoS probability and the UAV elevation angle is derived as (13), shown at the bottom of the next page, wherein the new parameter r_0 denotes the average building radius in a selected region and erf(·) is the error function.

III. RAY TRACING BASED SIMULATIONS

In this section, we describe the ray tracing-based simulations in detail. First, the deployment scenarios and parameters are introduced. Then we describe two simulations, LoS data-related simulations, and channel characteristic-related simulations respectively.

A. DEPLOYMENT SCENARIOS AND PARAMETERS

We first select four regions in New York City based on the open street map (OSM) to represent four different urban landscapes. Each region has a rectangular shape with a dimension of 840 × 450 m^2. The corresponding three-dimensional (3D) building maps are illustrated in Fig. 2 where four urban environments, namely, suburban, urban, dense urban, and high-rise urban are given. The average building heights in the four regions are 6.5 m, 12.2 m, 22.7 m, and 55.0 m, respectively. And the average building radius (the new parameter r_0 mentioned in II-B3) are 5.4 m, 9.3 m, 9.6 m, and 14.7 m for the four regions, respectively. First of all, we conducted an empirical analysis of the building height data obtained from the *New York City Open Data* [24] by using the 'Distribution Fitter Toolbox' in MATLAB, for the selected four regions. As seen from Fig. 3, for the CDF empirical data of building heights in the four regions, the log-normal distribution fits better than the Rayleigh distribution, especially for Regions 3 and 4.

TABLE 2. Environment parameters of four regions.

Regions/Parameters	α	β	γ
Region 1	0.26	2582.70	4.87
Region 2	0.43	1100.90	10.28
Region 3	0.94	2433.90	19.15
Region 4	0.78	844.00	54.07

The previously defined environmental parameters of the four regions are calculated as $\alpha = \frac{A_{\mathrm{bldg}}}{A_{\mathrm{tot}}}$ and $\beta = \frac{N_{\mathrm{bldg}}}{A_{\mathrm{tot}}}$ respectively. A_{bldg} and A_{tot} denote the area covered by buildings and the total selected area respectively, and N_{bldg} is the number of buildings in the selected area. The calculation of γ is the maximum likelihood estimation (MLE) of the Rayleigh parameter: $\gamma = \sqrt{\frac{1}{2n}\sum_{i=1}^{n} h_i^2}$. Where $n = N_{\mathrm{bldg}}$ and h_i denotes the height of the i-th building. In addition, the base area, number and height of buildings are obtained from *New York City Open Data* [24]. The calculated environmental parameters are shown in Table 2.

B. SIMULATION DESIGN

We conducted three types of ray-tracing simulations using the Communications Toolbox of MATLAB. The first two are the LoS data-related simulations based on the receivers on the one circle and multiple circles, respectively. These two simulations aim to study and verify the relationship between the LoS probability and the elevation angle of the UAV in four urban environments. The third one is to obtain the path loss and shadow fading characteristics of LoS and NLoS propagation in different urban environments. In particular, the RT simulation platform (PC) has a configuration of Intel® Core i7-11700F Processor (2.50 GHz) and a total RAM of 16 GB.

The format for invoking the ray tracing model is written as raytrace(tx, rx), where tx and rx are pre-defined transmitters and receivers' site objectives, respectively. The propagation paths are found using ray tracing with the terrain and

$$P_{LoS1}(\theta) = \prod_{i=0}^{n-1}\left[1 - \exp\left(-\frac{\left(d_{rx}\tan\theta - \frac{\left(i+\frac{1}{2}\right)d_{rx}\tan\theta}{n}\right)^2}{2\gamma^2}\right)\right] \quad (5)$$

buildings data defined in the site viewer map which is a given 3D environment based on the OSM map file used. The original OSM map can be obtained free of charge from the Open Street Map website. Additionally, a ray tracing propagation model can be created using the ''raytracing-image-method'', which is an option provided by the Communications Toolbox of MATLAB. The interaction types of this method option include effects from reflection and do not include effects from diffraction, refraction, or scattering, and the operational frequency for this function is from 100 MHz to 100 GHz, which suits our investigated carrier frequency at 28 GHz. Moreover, the ''raytracing-image-method'' supports up to two path reflections. In our ray-tracing simulation, the building material and terrain material are both set as concrete, due to the widespread use of this material in urban environments. The computational complexity of our ray-tracing simulation increases exponentially with the number of reflections.

1) PROBABILITY OF LoS SIMULATION BASED ON RECEIVERS ON ONE CIRCLE

First of all, for simulation consistency, we fix the same deployment scheme for the UAV and ground receivers in the four regions. Take the deployment in one region as an example, the projected coordinates of the UAV on the ground are at the center of the rectangular shape, and the height range is adjusted from 10 m to 500 m with a step of 5 m interval. The position of a receiver on the ground is placed on a circle of a 200-meter radius and the receiver's height is 1.5 m. It is worth noting that, as aforementioned in Sub-section II-A, the expression of the probability of LoS is valid under condition $d_{rx} \geq \frac{2}{\sqrt{\alpha\beta}}$. It is verified that this condition can be met when $d_{rx} \geq 200$ m in four urban environments.

In addition, the intrinsic nature of a statistical method requires the number of ground receivers as large as possible to guarantee the accuracy of the simulation results. We randomly deploy 5000 receivers on the circle with a 200-m radius, and hence these 5000 receivers may be on the ground or on the surface of a building. Since the receivers in the LoS expression should be those placed on the ground by default, we exclude the receivers that are not distributed on the ground. The numbers of ground receivers in the four regions of the simulation are 4121, 3434, 1901, and 2149, respectively. Next, we calculate the LoS/NLoS status of the propagation channel between the UAV and the ground receivers when the UAV stays at different heights in the four regions. Eventually, the obtained LoS/NLoS status data is presented in Fig. 4.

As illustrated, Fig. 4 demonstrates the changes in the LoS status between the UAV and ground receivers at different heights in the suburban, urban, dense urban, and high-rise urban environments respectively. The blue color represents the LoS status, and the red one stands for the NLoS status. It is easy to observe the intermittent blanks on the circumference of all four sub-figures, which is explained by the occupancy of buildings.

Finally, in the four areas, we calculate the ratio of the number of receivers operating in the LoS state (N_{LoS}) to the total number of receivers (N_{rx}) under different UAV elevation angles, and then the approximate value of the LoS probability can be obtained. The relationship between the calculated LoS probability of the UAV in the four regions and the elevation angle of the UAV will be given in Subsection IV-A. Additionally, due to the weaker statistical power when considering the receivers only in one circle, the analysis has been extended to multiple circles in the following paragraph.

2) PROBABILITY OF LoS SIMULATION BASED ON RECEIVERS ON MULTIPLE CIRCLES

The height of the UAV ranges from 10 to 500 meters with an interval of 10 meters, so there are fifty different heights of the UAV. Then we also set the ground receivers of fifty circles with the projection of the UAV on the ground as the center. The radius of these circles ranges from 4 to 200 meters with an interval of 4 meters. It is worth noting that although we mentioned that the LoS probability expression is valid when $d_{rx} \geq 200$ meters, this condition is only applicable for the ITU LoS probability expression. Consequently, comparing the LoS probability data obtained from our simulations (based on multiple circles) with the ITU's expression may not be suitable. Then, we placed various numbers of receivers on each circle, according to each circle's perimeter. The total number of receivers on the fifty circles in each region are 61523, 50863, 33466, and 34816, respectively. After conducting the RT simulations, we obtained and analyzed enormous LoS/NLoS status data from four regions and visualized them in a 3D manner as illustrated in Fig. 5.

$$V(d_{rx}) = \sqrt{\alpha\beta}\int_0^{d_{rx}} G(h_0)\,dl = \sqrt{\alpha\beta}\int_0^{d_{rx}} \left(\frac{1}{2} - \frac{1}{2}\,\mathrm{erf}\left[\frac{\ln h_0 - \mu_0}{\sqrt{2}\sigma_0}\right]\right) dl_d. \tag{10}$$

$$P_{LoS3} = \exp\left(-V(d_{rx})\right) = \exp\left(-\sqrt{\alpha\beta}\int_0^{d_{rx}} \left(\frac{1}{2} - \frac{1}{2}\,\mathrm{erf}\left[\frac{\ln h_0 - \mu_0}{\sqrt{2}\sigma_0}\right]\right) dl_d\right). \tag{11}$$

$$P_{LoS3}(\theta) = \exp\left(-\sqrt{\alpha\beta}\int_0^{d_{rx}} \left(\frac{1}{2} - \frac{1}{2}\,\mathrm{erf}\left[\frac{\ln\left((d_{rx} - l_d)\tan(\theta) + h_{rx}\right) - \mu_0}{\sqrt{2}\sigma_0}\right]\right) dl_d\right). \tag{12}$$

$$P_{LoS4}(\theta) = \exp\left(-\beta\int_0^{d_{rx}} \left(\frac{1}{2} - \frac{1}{2}\,\mathrm{erf}\left[\frac{\ln\left((d_{rx} - l_d)\tan(\theta) + h_{rx}\right) - \mu_0}{\sqrt{2}\sigma_0}\right]\right)\left(2r_0 - \sqrt{\max\left(4r_0^2 - l_d^2, 0\right)}\right) dl_d\right). \tag{13}$$

(a) Region 1. (b) Region 2.

(c) Region 3. (d) Region 4.

FIGURE 2. Four regions in New York city correspond to suburban, urban, dense urban and high-rise urban.

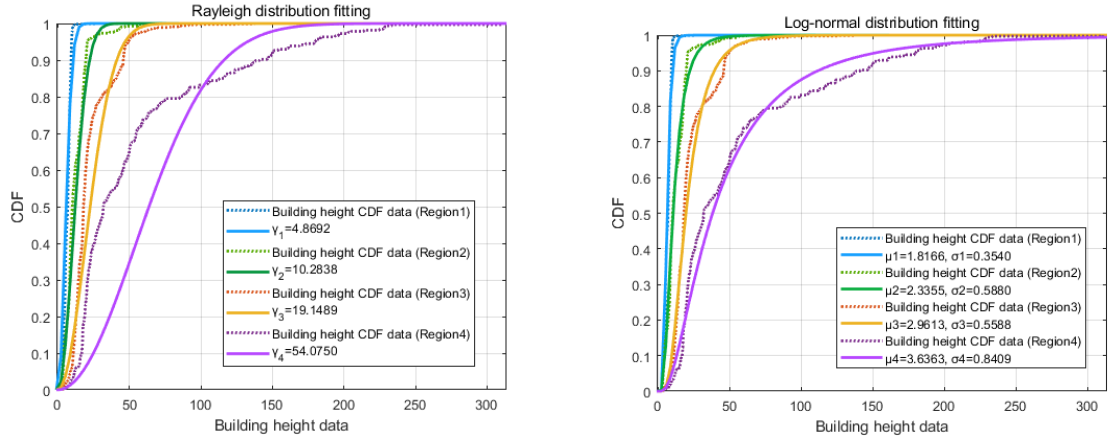

(a) (b)

FIGURE 3. Height distribution of buildings in four regions, comparing the empirical cumulative distribution function (CDF) data of the building heights with (a) the Rayleigh distribution model and (b) the log-normal distribution model.

As illustrated, Fig. 5 demonstrates the changes in the LoS status between the UAV and ground receivers on multiple circles at different heights in the suburban, urban, dense urban, and high-rise urban environments, respectively. The blue color represents the LoS status, and the red stands for the NLoS status. In the four regions, we first calculate the ratio of the number of receivers (operating in the LoS state) to the number of all receivers (N_{rx}) in each circle under different UAV elevation angles. Then, we average the LoS ratios corresponding to the same elevation angle on all circles to obtain the approximate probability value of LoS. The relationship of LoS probability versus elevation angle based on the simulations of receivers situated on multiple circles is given in subsection IV-B.

3) CHANNEL CHARACTERISTIC RELATED SIMULATION

The purpose of this simulation is to explore the path loss and shadow fading characteristics of LoS and NLoS based on the A2G ray tracing channel data in different urban environments. The vertically projected coordinate of the UAV on the ground is still set to the center of the region of rectangular shape, and the height of the UAV ranges from 15 m to 585 m (with a step of 30 m interval). The receivers are randomly distributed within a circular area with a radius of half the length of the short side of the rectangular shape, they are all placed at a height of 1.5 m. The number of the ground receivers in the suburban, urban, dense urban, and high-rise urban regions is 2435, 2031, 1256, and 1405, respectively. Moreover, the transmitter has an output power of 10 watts

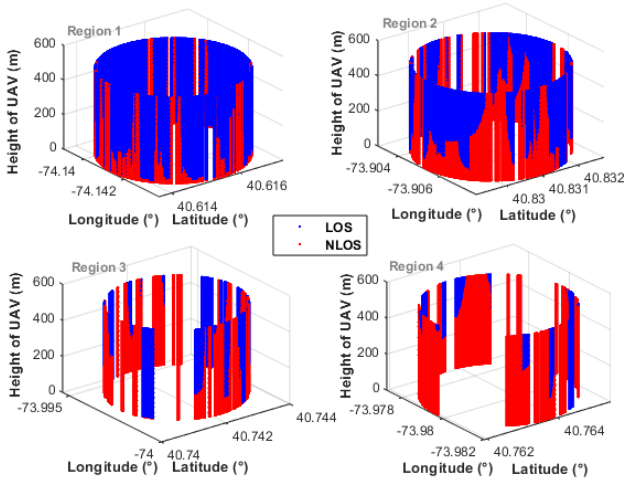

FIGURE 4. LoS/NLoS status between UAV and ground receivers on one circle in four regions.

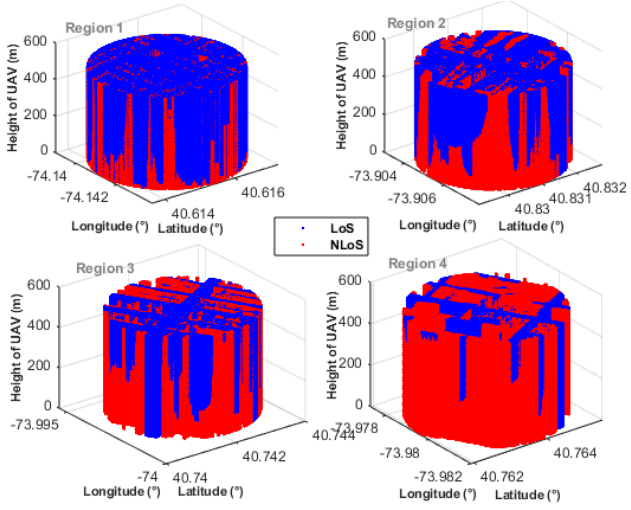

FIGURE 5. LoS/NLoS status between UAV and ground receivers on multiple circles in four regions.

(40 dBm), and it operates on the carrier frequency of 28 GHz. The bandwidth of all the ground receivers is set to 20 MHz with which we could calculate the noise floor to be -101 dBm. Both the transmitter and receiver antennas are isotropic. After completing the deployment of the UAV and the ground receivers, the path loss data can be extracted using the A2G ray tracing method. The equation for path loss is given by

$$PL(dB) = 20\log_{10}\left(\frac{4\pi d_0}{\lambda}\right) + 10n\log_{10}\left(\frac{d}{d_0}\right) + X_\sigma, \tag{14}$$

where d_0 is the reference distance and its value is usually from 10 m to 100 m for outdoor scenarios. λ is the wavelength, d denotes the distance from UAV to the receiver and n denotes the path loss exponent (PLE). X_σ is a Gaussian random variable with a mean value of zero and a variance of σ_{SF}^2 to represent the shadow fading. Furthermore, we use (14) without the last term to fit the extracted RT data to obtain the path loss

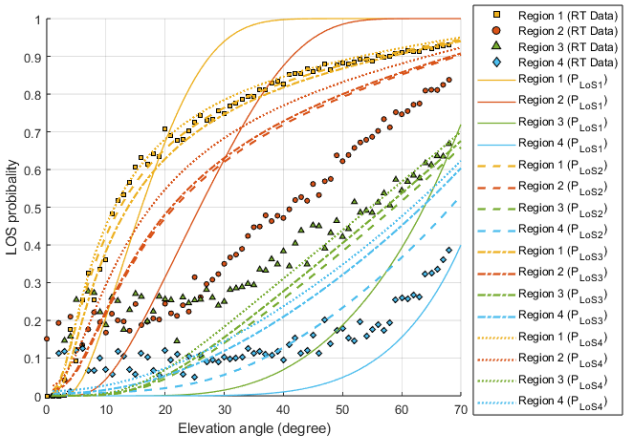

FIGURE 6. LoS probability comparison between the RT simulation data (based receivers located on one circle) and the theoretical expression in (5), (6), (12), and (13).

exponent, and the root mean square error (RMSE) of the fit is the standard deviation of the shadowing X_σ. The statistical analysis of LoS and NLoS shadow fading with various UAV deployment altitudes in the four regions will be demonstrated in Subsection IV-C.

IV. SIMULATION RESULTS

A. RESULTS OF THE LoS SIMULATION BASED ON RECEIVERS LOCATED ON ONE CIRCLE

This study compares the four theoretical formulas in subsections II-A and II-B to the RT simulation results in four regions. Specifically, we compare the LoS probability data based on simulations of ground receivers located on one single circle, with expressions (5), (6), (12), and (13). For expression (5), it is based on the assumption that the building heights follow the Rayleigh distribution and that the locations of the buildings are evenly spaced. Expressions (6), (12), and (13) have the same type of building location distribution, and their buildings are all modeled as random points following a Poisson point process (PPP). But these three expressions are based on different types of building heights' distribution. The building heights in expression (6) conform to the Rayleigh distribution, while the building heights in expressions (12) and (13) conform to the log-normal distribution.

As illustrated in Fig. 6 that the LoS expressions (5), (6), (12), and (13) are represented by the solid line, the dashed line, the dot-dash line, and the dotted line, respectively. It can be seen from Fig. 6 that the trend of LoS probability obtained from RT simulation data fits better to expressions (6), (12), and (13) than expression (5). However, except for the curves of expressions (6), (12), and (13) for Region 1, the others are still not ideal with visible discrepancies.

Furthermore, as illustrated in Fig. 6, the RT LoS probability data in Region 3 (dense urban) is higher than that in Region 2 (urban) when the elevation angle is less than around 25 degree which is unlike the theoretical result in (6). To further analyze this phenomenon, we have selected the LoS/NLoS data

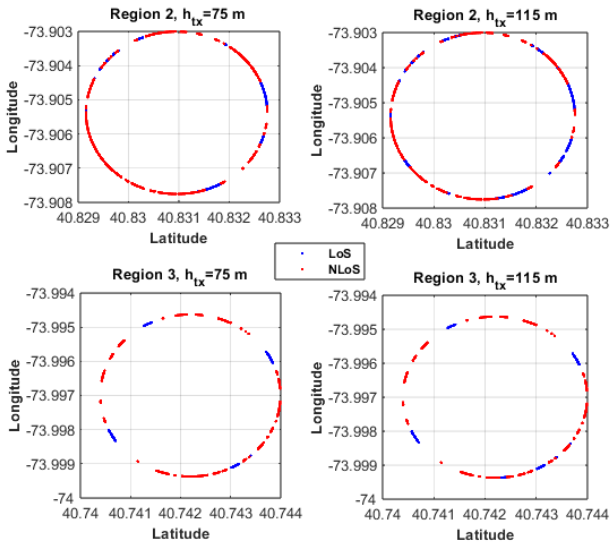

FIGURE 7. LoS/NLoS data comparison between Region 2 and Region 3.

of Region 2 and Region 3 when the elevation angle is less than 25 degree ($h_{tx} = 75$ m) and greater than 25 degree ($h_{tx} = 115$ m) for comparison. As illustrated in Fig. 7, the number of red points (representing the NLoS data) in Region 3 is smaller than that in Region 2. Note that, since the building density in Region 3 is significantly larger than that in Region 2 as shown in Table 2 and Fig. 2, and the number of receivers (indicated by all blue and red points) on the ground in Region 3 is smaller than that in Region 2. Therefore, the ratio of the blue LoS points to all points in Region 3 tends to be larger than that in Region 2. The difference in the average building height in Region 2 and Region 3 is less significant among all regions.

B. RESULTS OF THE LoS SIMULATION BASED ON RECEIVERS LOCATED ON MULTIPLE CIRCLES

In this subsection, we compare the simulated LoS probability data from the receivers at circles of different radii with the expressions (6), (12), and (13). The expression (5) is not taken into account due to its unsuitability at a radius smaller than 200 meters.

As illustrated in Fig. 8, the LoS expressions (6), (12), and (13) are represented by the dashed line, the dot-dash line, and the dotted line, respectively. As observed, for Region 1 and Region 2, the LoS probabilities data obtained from RT simulations are more fittable to the curves of expressions (6), (12), and (13), which is an improvement over its counterparts in Fig. 6. However, for other regions, the curves of expressions (6), (12), and (13) are still deviant from the RT simulation data.

Since the curves of the above three LoS probability expressions cannot perfectly fit the trends of the realistic RT simulation data, in this section, we present our own LoS probability expression and fitting curves as shown in Fig. 9. The elevation angle-dependent LoS probability expression is given as

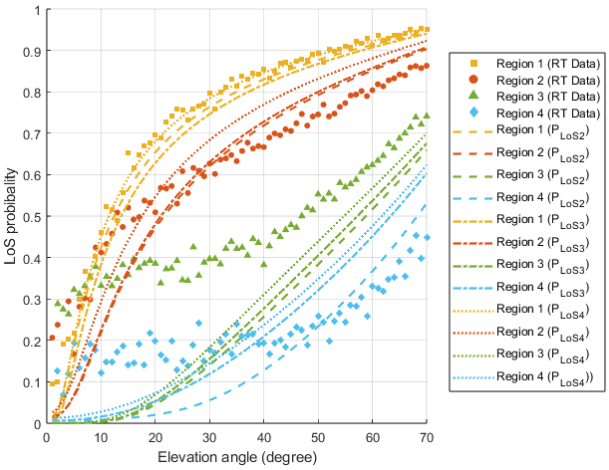

FIGURE 8. LoS probability comparison between the RT simulation data (based receivers located on one circle) and the theoretical expression in (6), (12), and (13).

TABLE 3. Parameters of the fitted curves in four regions.

Regions/Parameters	a	b	c	d
Region 1	0.7990	0.0025	-0.8094	-0.0810
Region 2	0.5093	0.0077	-0.3788	-0.0934
Region 3	0.1228	-0.0290	0.1985	0.0186
Region 4	0.1478	-0.0091	0.0128	0.0490

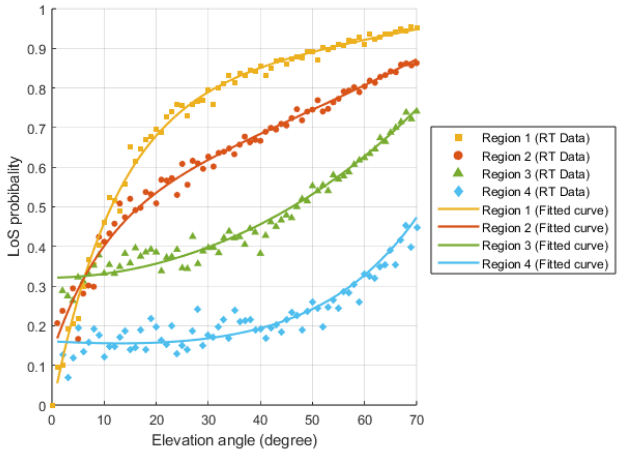

FIGURE 9. LoS probability versus elevation angle under exponential fitting curves, based on ray tracing data obtained from receivers on multiple circles.

follows

$$P_{LoS} = ae^{b\theta} + ce^{d\theta}, \left(0 \le \theta \le 70^{\circ}\right), \tag{15}$$

where the parameters a, b, c and d in the four regions are shown in Table 3 as follows.

It can be seen from Fig. 9 that our own proposed expression for the LoS probability based on the elevation angle well fits the trends of the RT simulation data in all four regions. The relationship between the four parameters in the LoS probability expression and the parameters of the urban environments will be dedicated in future research work.

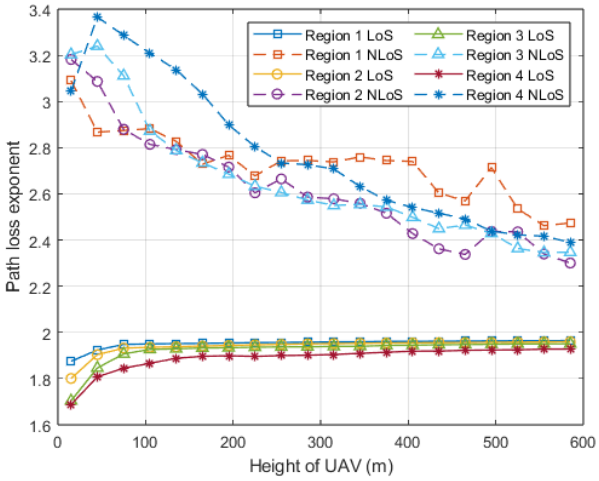

FIGURE 10. LoS and NLoS PLEs versus the height of UAV.

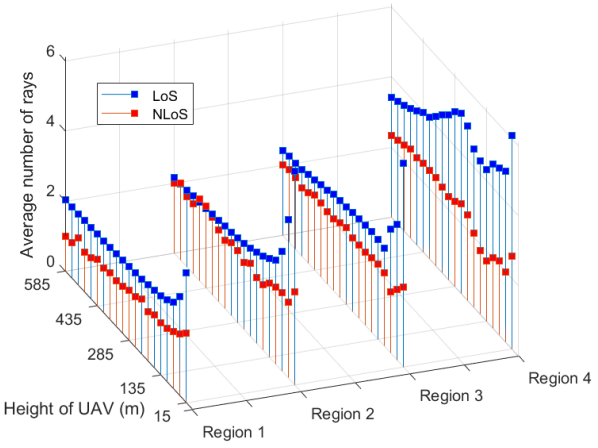

FIGURE 11. Average number of rays arrived at each receiver versus the height of UAV.

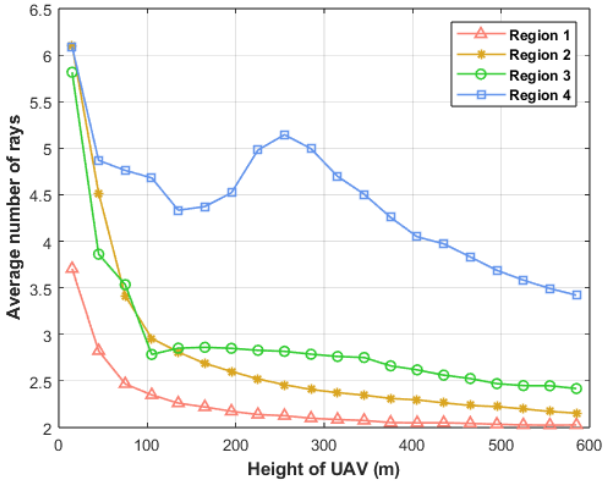

FIGURE 12. Average number of rays (which must include one LoS ray for each ground receiver) versus the height of the UAV (with a step of 30 m, from 15 m to 585 m).

C. RESULTS OF CHANNEL CHARACTERISTIC RELATED SIMULATION

The relationship between the PLE of LoS/NLoS obtained from the A2G RT data set and the UAV height is shown in Fig. 10 where the PLE of the LoS link changes more smoothly than that of the NLoS link. The former increases with the growth of the UAV height and gradually approach the value of 2, while the latter decreases from a high value to the free space exponent of 2 with the higher UAV height. In addition, when the UAV height is less than around 100 meters, the PLE of the LoS link in the four areas demonstrates an obvious upward growth with a steeper slope. This phenomenon can be explained that when the UAV flies at an altitude that is lower or close to the average building height of the corresponding region, the richness of reflections and the waveguiding effect can occur in the signal propagation. This waveguiding effect that causes the PLE smaller than 2 (free-space PLE) is also frequently seen in the indoor corridor wireless propagation measurement [23].

Furthermore, we analyze the relationship between the average number of rays received by each receiver in the four regions and the UAV height. As shown in Fig. 11, when the UAV height is less than around 100 meters, the average number of rays received by the receiver is significantly reduced as the height of the UAV increases. From the perspective of real urban environments, when the height of the UAV is less than around 100 meters, the aforementioned waveguiding effect is more obvious resulting in more rays to be received by the receiver, and vice versa.

Furthermore, we particularly investigate the ground receivers with LoS communication in the four regions and plot the average number of rays versus the UAV height in Fig. 12. As can be observed, Region 4 shows a very obvious fluctuation between 105 m and 255 m (UAV height), while Region 3 also demonstrates a tiny fluctuation from 105 m to 165 m. This is because, there are still rich reflectors in the propagation path (and environment) when the UAV flies lower than the highest buildings of the region (310 m and 137 m in Region 4 and Region, respectively), despite that the overall LoS communication probability monotonically increases as illustrated in Fig. 13. It is worth mentioning that, the LoS probability increment will enter the saturation region when the UAV flies significantly high.

The relationship between the standard deviation of shadow fading under LoS/Nlos conditions and various UAV deployment altitudes in the four regions is illustrated in Fig. 14. It can be observed that, being similar to Fig. 10, the standard deviation of shadow fading in LoS link changes smoother than that of NLoS as the drone height increases. Moreover, it demonstrates a comparatively flat curve with a slightly ascending order in terms of the increased complexity of the urban environment. Moreover, when the UAV height is lower than 100 m, the shadow fading standard deviation of the LoS link has a larger decreasing slope which can be explained by the waveguiding effect as a root cause which also leads to a series of observations under 100 m for both Figs. 10 and 11.

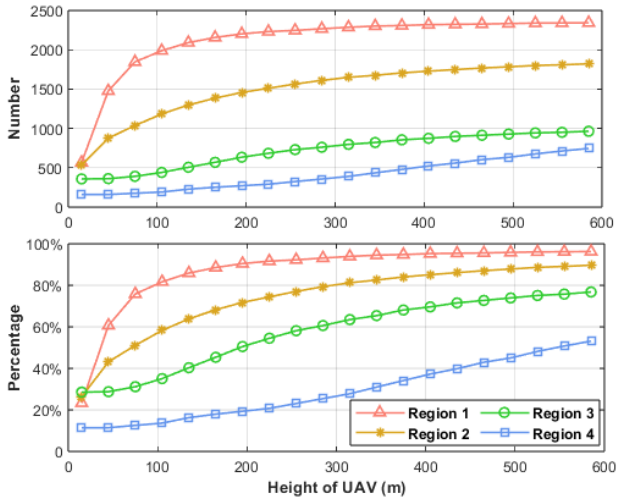

FIGURE 13. Number and the percentage of ground receivers, both holding LoS communication with the UAV, in four regions.

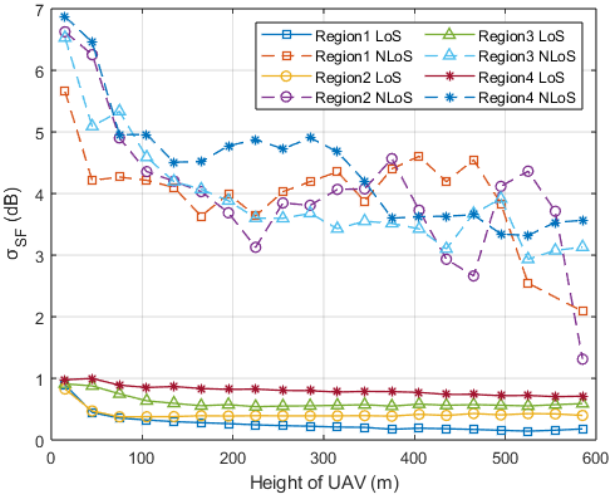

FIGURE 14. LoS and NLoS standard deviation of shadow fading versus the height of UAV.

V. CONCLUSION

In this paper, we have compared and verified four elevation angle-dependent probability expressions of LoS by conducting real-world urban environment-based simulations from the analysis of the extracted A2G ray tracing channel data. One of the most critical conclusions is that the elevation angle-dependent probability expression of LoS based on the assumption of randomly distributed buildings in the literature can better match and estimate the LoS probability between the UAV and the ground receivers in realistic urban environments. Moreover, based on the massive A2G ray tracing simulation data, we have unveiled the critical relationship between the UAV altitude and the A2G channel parameters such as the PLE and the standard deviation of the shadowing effect.

The future work includes several aspects, namely, the other characteristics of the A2G channel based on the realistic urban environment such as the Doppler effect in a highly dynamic environment; investigating various meteorological conditions and building materials that affect the UAV communications at high-frequency bands; UAV deployment strategy for various geological and weather conditions.

REFERENCES

[1] O. M. Bushnaq, A. Chaaban, and T. Y. Al-Naffouri, "The role of UAV-IoT networks in future wildfire detection," *IEEE Internet Things J.*, vol. 8, no. 23, pp. 16984–16999, Dec. 2021.
[2] Y. Huo, X. Dong, and S. Beatty, "Cellular communications in ocean waves for maritime Internet of Things," *IEEE Internet Things J.*, vol. 7, no. 10, pp. 9965–9979, Oct. 2020.
[3] V. N. Nguyen, R. Jenssen, and D. Roverso, "Intelligent monitoring and inspection of power line components powered by UAVs and deep learning," *IEEE Power Energy Technol. Syst. J.*, vol. 6, no. 1, pp. 11–21, Mar. 2019.
[4] E. Natalizio, N. R. Zema, E. Yanmaz, L. D. P. Pugliese, and F. Guerriero, "Take the field from your smartphone: Leveraging UAVs for event filming," *IEEE Trans. Mobile Comput.*, vol. 19, no. 8, pp. 1971–1983, Aug. 2020.
[5] M. Mozaffari, X. Lin, and S. Hayes, "Towards 6G with connected sky: UAVs and beyond," 2021, *arXiv:2103.01143*.
[6] Y. Huo, X. Dong, T. Lu, W. Xu, and M. Yuen, "Distributed and multilayer UAV networks for next-generation wireless communication and power transfer: A feasibility study," *IEEE Internet Things J.*, vol. 6, no. 4, pp. 7103–7115, Aug. 2019.
[7] X. You, C. X. Wang, J. Huang, X. Gao, Z. Zhang, M. Wang, Y. Huang, C. Zhang, Y. Jiang, J. Wang, and M. Zhu, "Towards 6G wireless communication networks: Vision, enabling technologies, and new paradigm shifts," *Sci. China Inf. Sci.*, vol. 64, no. 1, pp. 1–74, Nov. 2020.
[8] Y. Zeng, Q. Wu, and R. Zhang, "Accessing from the sky: A tutorial on UAV communications for 5G and beyond," *Proc. IEEE*, vol. 107, no. 12, pp. 2327–2375, Dec. 2019.
[9] M. Alzenad, A. El-Keyi, F. Lagum, and H. Yanikomeroglu, "3-D placement of an unmanned aerial vehicle base station (UAV-BS) for energy-efficient maximal coverage," *IEEE Wireless Commun. Lett.*, vol. 6, no. 4, pp. 434–437, Aug. 2017.
[10] X. Zhong, Y. Huo, X. Dong, and Z. Liang, "QoS-compliant 3-D deployment optimization strategy for UAV base stations," *IEEE Syst. J.*, vol. 15, no. 2, pp. 1795–1803, Jun. 2020.
[11] *Propagation Data and Prediction Methods Required for the Design of Terrestrial Broadband Radio Access Systems Operating in a Frequency Range From 3 to 60 GHz*, document Rec. ITU-R P.1410-5, Feb. 2012. [Online]. Available: https://www.itu.int/rec/R-REC-P.1410/en
[12] A. Al-Hourani, S. Kandeepan, and S. Lardner, "Optimal LAP altitude for maximum coverage," *IEEE Wireless Commun. Lett.*, vol. 3, no. 6, pp. 569–572, Dec. 2014.
[13] H. Kang, J. Joung, J. Ahn, and J. Kang, "Secrecy-aware altitude optimization for quasi-static UAV base station without eavesdropper location information," *IEEE Commun. Lett.*, vol. 23, no. 5, pp. 851–854, May 2019.
[14] X. Liu, J. Xu, and H. Tang, "Analysis of frequency-dependent line-of-sight probability in 3-D environment," *IEEE Commun. Lett.*, vol. 22, no. 8, pp. 1732–1735, Aug. 2018.
[15] Z. Cui, K. Guan, C. Briso-Rodriguez, B. Ai, and Z. Zhong, "Frequency-dependent line-of-sight probability modeling in built-up environments," *IEEE Internet Things J.*, vol. 7, no. 1, pp. 699–709, Jan. 2020.
[16] P. S. Bithas, V. Nikolaidis, A. G. Kanatas, and G. K. Karagiannidis, "UAV-to-ground communications: Channel modeling and UAV selection," *IEEE Trans. Commun.*, vol. 68, no. 8, pp. 5135–5144, Aug. 2020.
[17] M. Badi, J. Wensowitch, D. Rajan, and J. Camp, "Experimentally analyzing diverse antenna placements and orientations for UAV communications," *IEEE Trans. Veh. Technol.*, vol. 69, no. 12, pp. 14989–15004, Dec. 2020.
[18] M. Badi, S. Gupta, D. Rajan, and J. Camp, "Characterization of the human body impact on UAV-to-ground channels at ultra-low altitudes," *IEEE Trans. Veh. Technol.*, vol. 71, no. 1, pp. 339–353, Jan. 2022.
[19] A. Al-Hourani, "On the probability of line-of-sight in urban environments," *IEEE Wireless Commun. Lett.*, vol. 9, no. 8, pp. 1178–1181, Aug. 2020.
[20] M. Gapeyenko, D. Moltchanov, S. Andreev, and R. W. Heath, Jr., "Line-of-sight probability for mmWave-based UAV communications in 3D urban grid deployments," *IEEE Trans. Wireless Commun.*, vol. 20, no. 10, pp. 6566–6579, Oct. 2021.

[21] H. Kang, J. Joung, and J. Kang, "A study on probabilistic line-of-sight air-to-ground channel models," in *Proc. 34th Int. Tech. Conf. Circuits/Syst., Comput. Commun. (ITC-CSCC)*, Jun. 2019, pp. 1–2.
[22] M. J. Arpaio, E. M. Vitucci, M. Barbiroli, V. Degli-Esposti, D. Masotti, and F. Fuschini, "A multi-frequency investigation of air-to-ground urban propagation using a GPU-based ray launching algorithm," *IEEE Access*, vol. 9, pp. 54407–54419, 2021.
[23] M. K. Elmezughi, T. J. Afullo, and N. O. Oyie, "Performance study of path loss models at 14, 18, and 22 GHz in an indoor corridor environment for wireless communications," *SAIEE Afr. Res. J.*, vol. 112, no. 1, pp. 32–45, Mar. 2021.
[24] *New York City—Open Data Portal*. Accessed: Apr. 20, 2021. [Online]. Available: https://opendata.cityofnewyork.us/data/

MENGAN SONG (Student Member, IEEE) received the B.Eng. degree in information engineering from the Xi'an University of Posts and Telecommunications, China, in 2017. She is currently pursuing the Ph.D. degree with the School of Information, Chang'an University, China. The focus of her Ph.D. research is on wireless air-to-ground channel modeling for the next generation of communication systems. Her research interests include wireless channel modeling, millimeter-wave systems, and artificial intelligence. She is a Technical Reviewer of IEEE Access and IEEE VTC.

YIMING HUO (Senior Member, IEEE) received the B.Eng. degree in information engineering from Southeast University, China, in 2006, the M.Sc. degree in system-on-chip (SoC) from Lund University, Sweden, in 2010, and the Ph.D. degree in electrical engineering from the University of Victoria, Canada, in 2017.

He worked with Ericsson, ST-Ericsson, Chinese Academy of Sciences, STMicroelectronics, and Apple. He is currently a Research Associate with the University of Victoria. He holds several granted patents. His recent research interests include next-generation wireless systems and networks, the Internet of Things, space technology, astronomy, and artificial intelligence. He is an Organizing Committee Member of the IEEE Future Networks Massive MIMO Working Group. He was a recipient of multiple IEEE conference paper awards and the "Most Popular Article of IEEE Access," in 2017, and the ISSCC-STGA Award from the IEEE Solid-State Circuits Society (SSCS). He has served as the Program Committee/TPC for the IEEE ICUWB/IEEE VTC/IEEE ICC, the Session Chair for the IEEE 5G World Forum 2018, the Publication Chair for the IEEE PACRIM 2019, and the TPC Co-Chair/Publicity Co-Chair/Session Chair of IEEE Future Networks 1st Massive MIMO Workshop 2021/2022, and a technical reviewer for multiple premier IEEE conferences, and transactions/journals. He is an Associate Editor of IEEE Access and a Guest Editor of *Signals*.

ZHONGHUA LIANG (Senior Member, IEEE) received the B.Sc. degree in radio engineering and the M.Sc. and Ph.D. degrees in information and communication engineering from Xi'an Jiaotong University, Xi'an, China, in 1996, 2002, and 2007, respectively. From July 1996 to August 1999, he was with the Guilin Institute of Optical Communications (GIOC), Guilin, China, where he was a System Engineer in optical transmission systems. From 2008 to 2009, he was a Postdoctoral Fellow with the Department of Electrical and Computer Engineering, University of Victoria, Victoria, BC, Canada. Since 2010, he has been with the School of Information Engineering, Chang'an University, Xi'an, China, where he is currently a Professor. His research interests include ultra-wideband technology, wireless communication theory, the Internet of Things, wireless sensor networks, and adaptive signal processing techniques for wireless communication systems.

XIAODAI DONG (Senior Member, IEEE) received the B.Sc. degree in information and control engineering from Xi'an Jiaotong University, China, in 1992, the M.Sc. degree in electrical engineering from the National University of Singapore, in 1995, and the Ph.D. degree in electrical and computer engineering from Queen's University, Kingston, ON, Canada, in 2000.

From 1999 to 2002, she was with Nortel Networks, Ottawa, ON, Canada, and worked on the base transceiver design of the third-generation mobile communication systems. From 2002 to 2004, she was an Assistant Professor with the Department of Electrical and Computer Engineering, University of Alberta, Edmonton, AB, Canada. Since 2005, she has been with the University of Victoria, Victoria, BC, Canada, where she is currently a Professor with the Department of Electrical and Computer Engineering. Her research interests include 5G, mmWave communications, radio propagation, the Internet of Things, machine learning, terahertz communications, localization, wireless security, e-health, smart grid, and nano-communications. She was the Canada Research Chair (Tier II), from 2005 to 2015. She served as an Editor for IEEE Transactions on Wireless Communications, from 2009 to 2014, IEEE Transactions on Communications, from 2001 to 2007, and *Journal of Communications and Networks*, from 2006 to 2015. She is an Editor of the IEEE Transactions on Vehicular Technology and the IEEE Open Journal of the Communications Society.

TAO LU (Member, IEEE) received the B.Sc. degree from the Department of Physics, University of Manitoba, Winnipeg, MB, Canada, in 1995, the M.Sc. degree from the Department of Electrical and Computer Engineering, Queen's University, Kingston, ON, Canada, in 1998, and the Ph.D. degree from the Department of Physics, University of Waterloo, Waterloo, ON, Canada, in 2005. He worked in industry with various companies, including Nortel Networks, Ottawa, ON, Canada; Kymata, Ottawa; and Peleton, New York, NY, USA, on optical communications, from 1997 to 2001. Before joining the University of Victoria, Victoria, BC, Canada, he was a Postdoctoral Fellow with the Department of Applied Physics, California Institute of Technology, Pasadena, CA, USA, from 2006 to 2008. His research interests include optical microcavities and their applications to ultra narrow linewidth laser source, and bio-nano photonics. He is currently extending his research on machine learning algorithms with applications to spectral analysis, the Internet of Things, and indoor localization.